RSC Advances

PAPER

View Article Online
View Journal | View Issue

Check for updates

Cite this: *RSC Adv.*, 2023, **13**, 15554

Preparation of a phenylboronic acid and aldehyde bi-functional group modified silica absorbent and applications in removing Cr(VI) and reducing to Cr(III)

Qianyi Song, Mengqi Cheng, Hongxu Liu, Haijiao Jia, Yaqin Nan, Wenqing Zheng, Youxin Li * and James J. Bao

Received 27th March 2023
Accepted 16th May 2023

DOI: 10.1039/d3ra02009f

rsc.li/rsc-advances

Cr(VI) is a great threat to the ecological environment and human health, so it is urgent to remove Cr(VI) from the environment. In this study, a novel silica gel adsorbent SiO_2–CHO–APBA containing phenylboronic acids and aldehyde groups was prepared, evaluated and applied for removing Cr(VI) from water and soil samples. The adsorption conditions including pH, adsorbent dosage, initial concentration of Cr(VI), temperature and time were optimized. Its ability in removing Cr(VI) was investigated and compared with three other common adsorbents, SiO_2–NH_2, SiO_2–SH and SiO_2–EDTA. Data showed SiO_2–CHO–APBA had the highest adsorption capacity of 58.14 mg g^{-1} at pH 2 and could reach adsorption equilibrium in about 3 h. When 50 mg SiO_2–CHO–APBA was added in 20 mL of 50 mg L^{-1} Cr(VI) solution, more than 97% of Cr(VI) was removed. A mechanism study revealed that a cooperative interaction of both the aldehyde and boronic acid groups is attributed to Cr(VI) removal. The reducing function was gradually weakened with the consumption of the aldehyde group, which was oxidized to a carboxyl group by Cr(VI). This SiO_2–CHO–APBA adsorbent was successfully used for the removal of Cr(VI) from soil samples with satisfactory results which indicates a good potential in agriculture and other fields.

Open Access Article. Published on 23 May 2023. Downloaded on 2/13/2026 7:31:57 AM.
This article is licensed under a Creative Commons Attribution-NonCommercial 3.0 Unported Licence.

1. Introduction

Water pollution with toxic metal ions has become one of the most serious environmental problems.[1] Those toxic metal ions enter water through human activities and natural pathways, posing a threat to human health.[2] Chromium is a common metal and is widely used in diverse industrial processes, including the metal industry, electroplating, leather processing, cooling tower blowdown, dyeing and pigment synthesis.[3–5] Hexavalent (VI) and trivalent (III) are the main existing valences of chromium. Cr(VI) is more toxic and mobile compared to Cr(III), and is 100 times more toxic than Cr(III).[6,7] Cr(VI) is carcinogenic and mutagenic to living organisms and even if Cr(VI) is present in very low concentrations, it can also cause skin dermatitis, kidney damage, respiratory sensitization, and carcinogenicity to humans,[8–10] so it is urgent to remove Cr(VI) from waste water.[5] The maximum discharge limit of Cr(VI) to the aquatic environment is 1 mg L^{-1} in EU Member States.[11] In drinking water, the United States Environmental Protection Agency identified it as a Group A contaminant and set the maximum contaminant limits for total chromium of 100 μg L^{-1} in 1991,[9] and the World Health Organization required that the content must not exceed 50 μg L^{-1}.[12–14]

To date, chemical methods, biological methods, and physical methods have been developed for the elimination of the Cr(VI) from aqueous solutions, such as reduction and neutralization precipitation, electrochemical processes, photocatalysis, ion exchange, membrane separation and adsorption methods.[15–19] The most common conventional method for Cr(VI) removal is reduction to Cr(III) at acid condition and precipitated to $Cr(OH)_3$ under alkaline conditions. However, the disadvantage of the method is that it will generate solid waste, while is easy to cause secondary pollution. The electrochemical method has a high consumption of electricity, more side-reactions and is not suitable for the treatment of wastewater with low concentration of heavy metal ions. The big problem of ion exchange and membrane separation method is that it is difficult to avoid contamination to the membrane and the equipment maintenance cost is very high. Nowadays, adsorption has become by far the most versatile and widely used technology. Adsorption is considered as the most promising method due to its high efficiency, easy to operate, economical, renewable, and technological feasibility.[20,21] Numerous adsorbents including silica gel,[10,22] various types of nanomaterials,[23–25] nanofibers,[19,26] biochar,[20,27] hydrogel,[28] functionalized polymers,[8,29] metal

Tianjin Key Laboratory for Modern Drug Delivery and High-Efficiency, Collaborative Innovation Center of Chemical Science and Engineering, School of Pharmaceutical Science and Technology, Tianjin University, Tianjin 300072, China. E-mail: lyx@tju.edu.cn; Tel: +86-22-2789-2820

© 2023 The Author(s). Published by the Royal Society of Chemistry

Open Access Article. Published on 23 May 2023. Downloaded on 2/13/2026 7:31:57 AM.
This article is licensed under a Creative Commons Attribution-NonCommercial 3.0 Unported Licence.

composite[30] and metal–organic frameworks[31] have been used for Cr(VI) removal.

On top of the selection of base materials, surface modification can be used as an efficient means of improving the effectiveness of adsorption of the selected material. After modification, the number of binding sites in the adsorbents can be enhanced and thereby the adsorption capacity is increased.[32] Many compounds can be used to modify the adsorbent. For example, organic materials such as nitrogen-containing groups,[33,34] inorganic materials,[35,36] biological materials,[37,38] ionic liquid materials,[39] polymeric materials[23,40] have all been used for absorbent surface modifications. The combination of surface modified and adsorption methods for the removal of heavy metals from the environment has been the subject of many studies. For example, JinHyeong Lee,[33] Shunquan Shi,[20] Joanna, Dobrzyńska[1] had chosen amino groups as modified functional groups on mesoporous silica, magnetic biochar, and SBA-15 surfaces respectively for exploring the removal of Cr(VI) from solution. Wachiraporn Kettum[34] prepared boronic acid-functionalized carbon-based adsorbent, which showed good adsorption of Cu(II), Ni(II), and Cr(VI) ions. Huihui Mao[35] modified TiO_2 on the surface of silica-pillared clay and investigated the adsorption of Cr(VI), which showed very high efficiency and sensitivity for removing Cr(VI). However, most of the aforementioned compounds was used to generate a single functional group with the exception that a few of them multiple functional, such as the thiol/amino bi-functionalized adsorbent,[41] mercaptopropyl and ethylenediamine triacetate-modified silica gels,[3] thiol/sulfonic acid bi-functionalized materials,[42] and amino/carboxyl bi-functionalized adsorbent.[43] Compared to single functional group modifications, bifunctional group modifications are more effective as in the removal of Cr(VI).

In this paper, a novel phenylboronic acid and aldehyde modified bifunctional absorbent (SiO_2–CHO–APBA) was proposed and prepared. After a series of characterizations, the SiO_2–CHO–APBA was used to remove Cr(VI) and reduce part of it to Cr(III) for the first time. Its adsorption mechanism, adsorption kinetics, isotherms, and relating parameters such as pH, temperature, amount of adsorbent, time and initial concentration of Cr(VI) were investigated. Its absorption ability to Cr(VI) was evaluated and compared with the other three common absorbents. Finally, this adsorbent was used in removal of Cr(VI) in soil.

2. Materials and methods

2.1 Materials

Thin-layer chromatography (TLC) grade silica gel purchased from Qingdao Haiyang Chemical Plant (Shandong, China) was used as the base material of the adsorbents. Toluene, diethyl ether absolute and hydrochloric acid (HCl, 36–38%) were from Rionlon Pharmaceutical Chemical Co., Ltd (Tianjin, China). Anhydrous ethanol was from Jiangtian Chemical Technology Co., Ltd (Tianjin, China). Acetone and phosphoric acid (H_3PO_4, 98%) were from Bohua Chemical Reagent Co. Ltd (Tianjin, China). Dichloromethane and hydroxylamine hydrochloride (H_2N–OH·HCl) were from Jindongtianzheng Precision Chemical Reagent Factory (Tianjin, China). Sulphuric acid (H_2SO_4, 95–98%), sodium hydroxide (NaOH, 96%) and potassium persulfate ($K_2S_2O_8$, 99.5%) were from Damao Chemical Reagent Factory (Tianjin, China). Disodium hydrogen phosphate (Na_2HPO_4, 99%), sodium dihydrogen phosphate (NaH_2PO_4, 97%), 3-aminopropyltriethoxysilane (APTES, 98%), and 3-aminophenylboronic acid (APBA, 98%) were from Heowns Biochem Technology (Tianjin, China). Glutaraldehyde (GA, 25% water solution) was from Kermel Chemical Reagent Co., Ltd (Tianjin, China). Sodium cyanoborohydride ($NaBH_3CN$, 95%) and 1,5-diphenylcarbohydrazide (DPC, 98%) were from Meryer Chemical Technology Co., Ltd (Shanghai, China). Potassium dichromate ($K_2Cr_2O_7$, 99.8%) was from Tianjin North Chemical Glass Purchase and Sales Center (Tianjin, China). Catechol (99.5%) was from Rhawn Chemical Technology Co., Ltd (Shanghai, China). All these chemicals were analytical grade and used without further purification. Ultrapure water was obtained in-house through a SCI-10-B Ultra-pure water system from Kerun Water Treatment Equipment Co., Ltd (Chongqing, China). The mercaptopropyl-functionalized silica gel (SiO_2–SH) and carboxyl functionalized silica gel (SiO_2–EDTA) were purchased from Anhui Biomics Biopharmaceutical Research Institute Co., Ltd (Anhui, China).

2.2 Instruments

A series of instruments were used to characterize SiO_2–CHO–APBA and its intermediates. Fourier-transform infrared spectra were analyzed with a TENSOR 27 FT-IR Spectroscopy (Bruker, Germany) by the KBr method. The morphology of SiO_2–CHO–APBA was characterized by Nanosem 430 Field emission scanning electron microscope (FEI, USA) and JEM100CXII transmission electron microscope (JEOL, Japan). Its specific surface was measured using a Brunauer–Emmett–Teller surface area analyzer with NAVO Station (Quantachrome, USA) based on the nitrogen adsorption and desorption method. The content of B element in SiO_2–CHO–APBA was determined by inductively coupled plasma mass spectrometer (Agilent 5110, USA). Thermal analysis of SiO_2–CHO–APBA was carried out with a TGA 550 analyzer (Discovery, USA) under N_2 flow at a heating rate of 10 °C min^{-1} in the range of 30–600 °C. The concentration of Cr(VI) and Cr(III) in the supernatant was measured by Cary 60 UV-Vis spectrophotometer (Agilent, USA).

2.3 Preparation of boronic acid and aldehyde bifunctional groups modified absorbent

2.3.1 Preparation of amino-modified silica gel (SiO_2–NH_2). Silica gel of 50 g was dispersed in 200 mL 6 mol L^{-1} HCl and stirred at 60 °C. After 6 h, it was taken out and washed with ultrapure water to neutral and dried in vacuum oven overnight. The silica gel was activated in a vacuum oven at 130 °C for 3 h. The activated silica gel of 10 g was dispersed in 50 mL anhydrous toluene. After adding 12 mL APTES, the mixture was stirred for 24 h at 110 °C. The product was washed by toluene, anhydrous ethanol, acetone in turns three times. After drying, SiO_2–NH_2 was obtained.

Open Access Article. Published on 23 May 2023. Downloaded on 2/13/2026 7:31:57 AM. This article is licensed under a Creative Commons Attribution-NonCommercial 3.0 Unported Licence.

2.3.2 Preparation of SiO_2–CHO–APBA. Phosphate buffer solution (PBS, 0.1 mol L^{-1}, pH 7.4) was prepared from NaH_2PO_4 and Na_2HPO_4. SiO_2–NH_2 of 2.5 g was added into a mixture of 40 mL PBS buffer solution (0.1 mol L^{-1}, pH 7.4) and 10 mL of 25% glutaraldehyde. After adding 1 mL $NaBH_3CN$ of 0.1 mg mL^{-1} and 6 h of machinery stir (400 rpm) at room temperature, red solid of aldehyde modified silica gel (SiO_2–CHO) was filtrated and washed with distilled water. The SiO_2–CHO was placed in vacuum oven until dry. SiO_2–CHO of 1.0 g was dispersed in 50 mL 0.1 mol L^{-1} PBS solution (pH 7.4). APBA of 400 mg and $NaBH_3CN$ of 200 mg were added and the mixture was stirred (400 rpm) for 6 h at room temperature. The final product was washed by dichloromethane, acetone and diethyl ether in turns three times. After drying, SiO_2–CHO–APBA was obtained. The synthetic route of SiO_2–CHO–APBA was shown in Fig. 1.

2.4 Determination of bi-functional group content

The adsorption of Cr(VI) mainly relies on the participation of aldehyde and boronic acid functional groups on the material surface. Thus, the content of both functional groups is important for the adsorption effect.

To characterize the prepared SiO_2–CHO–APBA, the content of aldehyde and boronic acid were determined. The determination principle of aldehyde group is indirect titration.[44] Firstly, hydroxylamine hydrochloride (H_2N–OH·HCl) react with the aldehyde group which will produce oxime and hydrochloric acid. Then, sodium hydroxide is used to titrated the produced HCl. In this paper, 20 mg of SiO_2–CHO–APBA were accurately weighed and transferred into tube. After adding 10 mL of 0.25 mol L^{-1} H_2N–OH·HCl solution and 2 drops of 0.05% methyl orange as indicator, the tube was shaken for 2 h. Then, 5 mL of supernatant was taken out and titrated by 0.03 mol L^{-1} NaOH solution until the color change from red to yellow and no fading within 30 min. The analytical blank was parallel performed by replacing SiO_2–CHO–APBA with SiO_2–NH_2, recording the volume of NaOH consumed and all experiments were in parallel three times.

The content of the aldehyde group (mmol g^{-1}) was calculated by the following eqn (1):

$$Q = \frac{2 \times (V_1 - V_0) \times C_{NaOH}}{m} \quad (1)$$

where V_0 and V_1 are the volume (mL) of NaOH in blank and experimental group respectively, C_{NaOH} is the concentration (mol L^{-1}) of NaOH and m is the mass (g) of SiO_2–CHO–APBA.

The determination principle of the boronic acid group is that boronic acid can bind specifically with *cis*-diol. Catechol has a *cis*-diol structure and has a maximum absorption wavelength at 275 nm, which can be used for quantitative calculations. In this paper, 0.35 mg mL^{-1} catechol solution was prepared with 1/15 mol L^{-1} pH 8.5 NaH_2PO_4–Na_2HPO_4 solution. SiO_2–CHO–APBA of 25 mg and 10 mL catechol solution of 0.35 mg mL^{-1} were added into centrifuge tube and shaken for 4 h. After adsorption, the supernatant solution was diluted and determined by UV-Vis spectrophotometer. A series of different concentration catechol standard solutions (0.014, 0.0175, 0.021, 0.0245, 0.028, and 0.035 mg mL^{-1}) were prepared for the standard curve. All of processes were protected from light and all experiments were in parallel three times.

The content of the boronic acid group (mmol g^{-1}) was calculated by the following eqn (2):

$$Q = \frac{(C_0 - C_e) \times V}{m \times M} \quad (2)$$

where C_0 and C_e are the concentrations (mg mL^{-1}) of initial and equilibrium catechol solution, respectively. V is the volume (mL) of catechol solution and m is the mass (g) of SiO_2–CHO–APBA. M is the molar mass (g mol^{-1}) of catechol.

2.5 Adsorption and reduction of SiO_2–CHO–APBA to Cr(VI)

The stock solution of 10 mg mL^{-1} Cr(VI) was prepared by dissolving 0.2828 g of $K_2Cr_2O_7$ into 10 mL of ultrapure water and the stock was diluted to get different concentrations of Cr(VI) testing solutions. H_3PO_4, NaH_2PO_4, and Na_2HPO_4 were used to adjust the pH because they can form a series of phosphate buffer solutions and maintain the pH stability of the system.

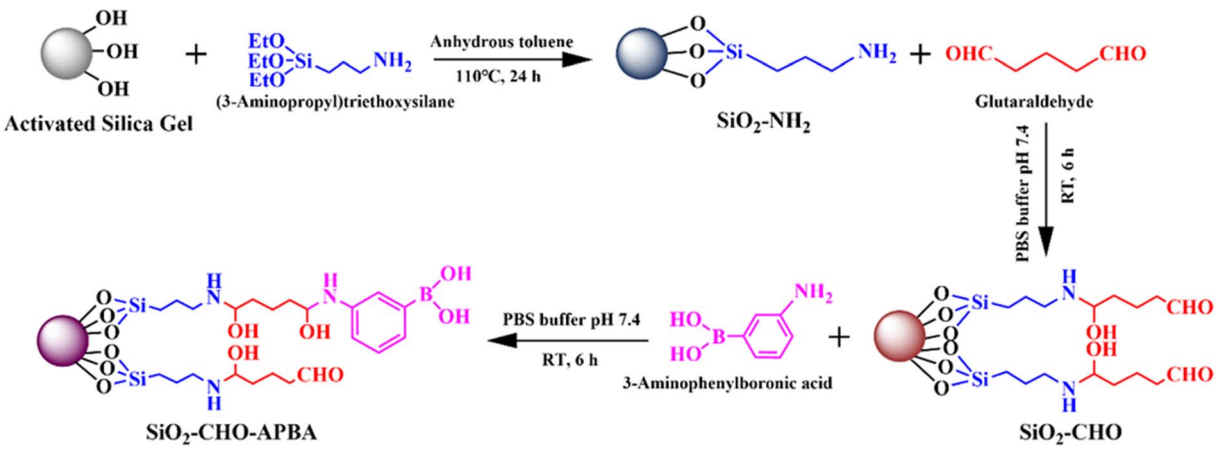

Fig. 1 The synthetic route of SiO_2–CHO–APBA.

© 2023 The Author(s). Published by the Royal Society of Chemistry

Open Access Article. Published on 23 May 2023. Downloaded on 2/13/2026 7:31:57 AM. This article is licensed under a Creative Commons Attribution-NonCommercial 3.0 Unported Licence.

Batch adsorption experiments were conducted in a temperature-controlled water bath shaker at 200 rpm. The concentration of Cr(VI) was measured according to the 1,5-diphenylcarbohydrazide colorimetric (DPC) method.[45] Its principle is that Cr(VI) can reacted with DPC to form Cr(VI)–DPC purple complexes under acidic condition, which can be quantified by UV-Vis (λ_{max} 540 nm). In this paper, H_2SO_4 of 50 mL, H_3PO_4 of 50 mL and ultrapure water of 100 mL were mixed well to obtain the acid solution. DPC solution was prepared through dissolving 0.2 g DPC in 50 mL of acetone and diluting to 100 mL using the above acid solution. Then, 500 μL of Cr(VI) sample and 1 mL of DPC solution were added to 25 mL colorimetric tube and diluted to 25 mL using ultrapure water. The mixture was stood for 10 min and measured at 540 nm. The concentration of Cr(III) is obtained by the difference between the total chromium concentration and the Cr(VI) concentration. Oxidation method was used to determine the total chromium content.[44,46] The sample solution containing chromium was taken in a test tube, 10 mL of ultrapure water and 200 μL of 5% potassium persulfate ($K_2S_2O_8$) were added and boiled for 20 min to oxidize Cr(III) to Cr(VI). The cooled solution was transferred to a 25 mL colorimetric tube, derivatized and determined according to the DPC method.

In order to optimize Cr(VI) adsorption conditions, the effect of initial pH, initial Cr(VI) concentration, time, temperature and amount of adsorbents were investigated. Cr(VI) solution of 20 mL was mixed with adsorbents (20–50 mg) at different pH value (2–8) with different concentration (5–200 mg L^{-1}) and temperature (20–70 °C) for different time (5–720 min).

The amount of the Cr(VI) adsorbed (mg g^{-1}) was calculated by the following eqn (3):

$$Q_t = \frac{(C_0 - C_e) \times V}{m} \quad (3)$$

The removal rate of the Cr(VI) (%) was calculated by the following eqn (4):

$$\text{Removal rate } (\%) = \frac{C_0 - C_e}{C_0} \times 100\% \quad (4)$$

where C_0 and C_e are the initial and equilibrium Cr(VI) concentrations (mg L^{-1}), respectively, V is the volume (mL) of initial solution and m is the mass (mg) of adsorbent.

2.6 Regeneration and reuse of SiO_2–CHO–APBA

The regeneration performance of the adsorbents is one of the important criteria to evaluate the applicability of the adsorbents. For desorption investigation, the Cr(VI)-adsorbed to SiO_2–CHO–APBA in 0.2 mol L^{-1} Na_3PO_4 solution was desorbed at 200 rpm for 4 h at 20 °C. The adsorption–desorption process of the same SiO_2–CHO–APBA was repeated five times to test the repeatability.

The desorption rate of the Cr(VI) (%) was calculated by the following eqn (5):

$$\text{Desorption rate}(\%) = \frac{C_d \times V_d}{V \times (C_0 - C_e)} \times 100\% \quad (5)$$

where C_d and V_d are the concentrations (mg L^{-1}) and volume (mL) of the desorbed Cr(VI) solution, respectively, V, C_0 and C_e are same as eqn (4).

3. Results and discussion

3.1 Characterization

The FT-IR results were shown in Fig. 2(a). We could observe the stretching vibration of –OH at 3450 cm^{-1}, asymmetric stretching vibration of Si–O–Si appeared at 1090 cm^{-1} and Si–OH bending bands between 800 cm^{-1}, which were consistent with report.[47] The peaks at 2945 cm^{-1} and 2879 cm^{-1} in the spectrum of SiO_2–NH_2 were attributed from the asymmetric and symmetric stretching vibration of methylene.[25,48] It indicated that the aminopropyl was successfully bonded which could provide the amino site for the next reaction.[49] After glutaraldehyde modification, a new band at 1681 cm^{-1} in IR spectrum of SiO_2–CHO was observed, which represented the presence of aldehyde groups.[47,50,51] The peak at 1446 cm^{-1} in IR spectrum of SiO_2–CHO–APBA which was the skeleton vibration of benzene ring.[52] The peak at 1357 cm^{-1} was from the B–O stretching vibration, which was the characteristic absorption peak of boronic acid group.[53] These indicated the phenylboronic acid had been bonded to SiO_2–CHO.

The adsorption and desorption isotherms of N_2 and the pore size distribution curve of SiO_2–CHO–APBA were shown in Fig. 2(b). Based on the adsorption isotherm classification of the IUPAC, the N_2 adsorption of SiO_2–CHO–APBA was a typical IV isotherm.[54,55] Its hysteresis loop appeared between 0.45 and 0.90 which belonged to H1-type with disordered pores.[54] The pore size of 6.56 nm and the narrow range of between 3.05 and 12.42 nm indicated SiO_2–CHO–APBA with mesopores.[25] The Brunauer–Emmett–Teller specific surface area of SiO_2–CHO–APBA calculated from the nitrogen adsorption analysis was 194.34 m^2 g^{-1}.

The morphology and structure of the SiO_2–CHO–APBA were observed by scanning electron microscope (SEM), and the results were shown in Fig. 2(c) and (d). It was obvious that SiO_2–CHO–APBA was irregular shape and the particle size was 30–100 μm. After increasing the magnification, it could be seen the surface was rough and uneven due to pores and concavities, which could effectively provide a large number of adsorption sites and facilitated the adsorption of targets. Transmission electron microscope (TEM) was used to observe the microstructural characteristics of the adsorbent (shown in Fig. 2(e)). The light and dark images indicated the existence of pores in the SiO_2–CHO–APBA.

The content of aldehyde group on the surface of SiO_2–CHO–APBA was 0.8074 mmol g^{-1} by the oxime reaction of aldehyde with H_2N–OH·HCl. The content of boronic acid group was measured as 0.1257 mmol g^{-1} by the affinity interaction of boronic acid with *cis*-diol. The B content from ICP-MS was 0.24% which was corresponding to 0.2233 mmol g^{-1}. These indicated that both functional groups were successfully bonded to the surface of the material.

TGA curve of SiO_2–CHO–APBA was shown in Fig. 2(f). From the data, a weight loss of 1.04% for the material was observed in

Open Access Article. Published on 23 May 2023. Downloaded on 2/13/2026 7:31:57 AM.
This article is licensed under a Creative Commons Attribution-NonCommercial 3.0 Unported Licence.

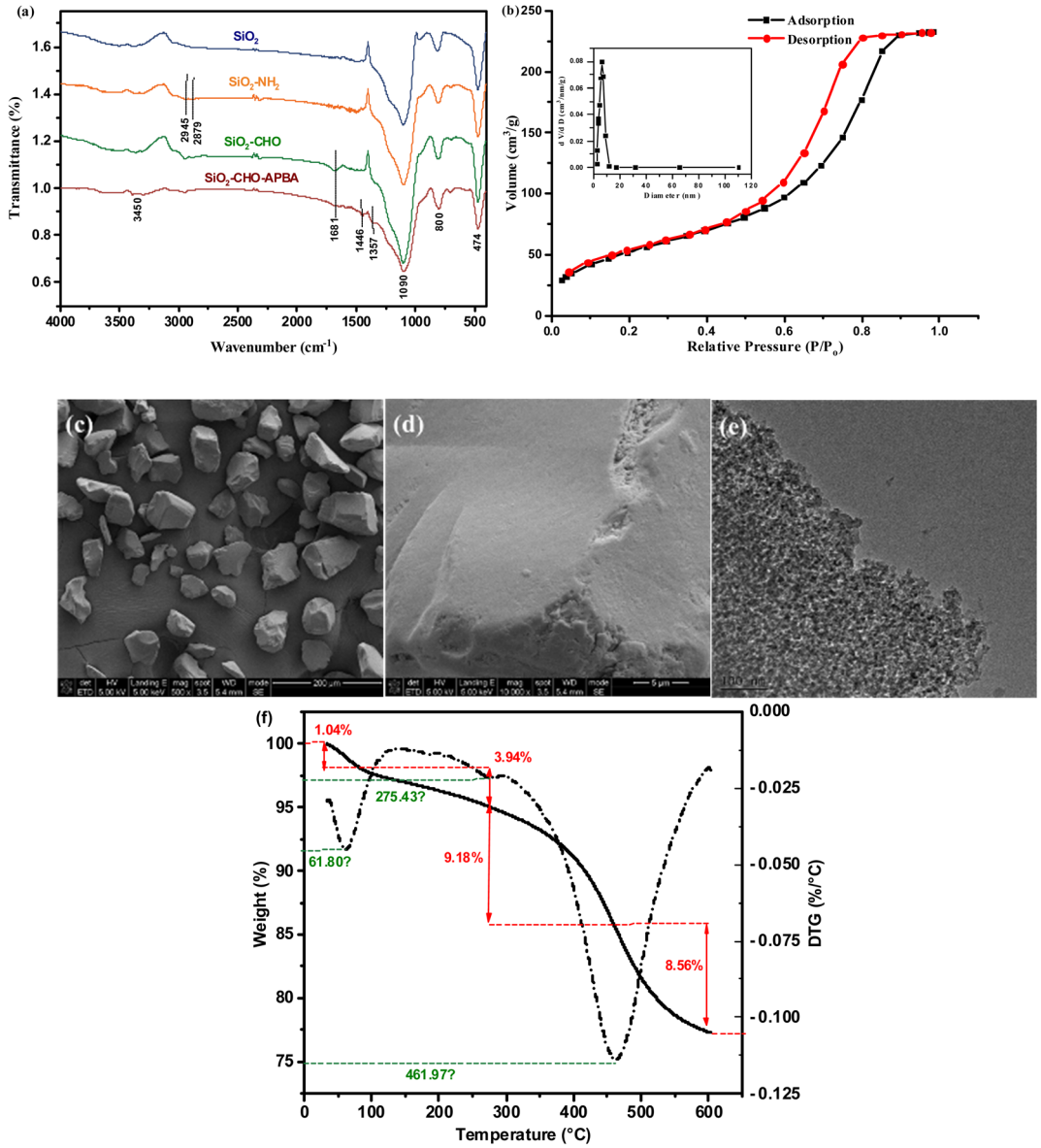

Fig. 2 (a) The FT-IR spectra of SiO_2–CHO–APBA and its intermediates; (b) nitrogen adsorption–desorption isotherm of SiO_2–CHO–APBA; (c) and (d) the SEM images of SiO_2–CHO–APBA; (e) the TEM image of SiO_2–CHO–APBA; (f) the TGA curve of SiO_2–CHO–APBA.

the range of 30–61.80 °C due to water evaporation.[56] A weight loss of 3.94% observed in the range of 61.80–275.43 °C was attributed to the loss of boronic group, which was higher than the boiling point of phenylboronic acid (265.9 °C).[57] There was a weight loss of 9.18% in the range of 275.43–460.64 °C which may be attributed to the degradation of decomposition of the amino-propyl group on the surface.[58] As the temperature up to 600 °C and continued to lose weight 8.56%, presumably due to dehydration condensation of the –OH on the silica gel surface.[59] The SiO_2–CHO–APBA was thermostable under low temperature.

3.2 Evaluation of SiO_2–CHO–APBA

3.2.1 Effect of pH on absorption of SiO_2–CHO–APBA to Cr(VI). As we known, the initial pH value has a significant impact on the adsorption process, because it can affect the surface charge of the adsorbents[22] and the presence form of chromium ions in the solution. Under strong acidic environment (pH < 2), Cr mainly exists as H_2CrO_4. In the range of pH 2–6, $HCrO_4^-$ co-exists as $Cr_2O_7^{2-}$ from hydrolysis of $HCrO_4^-$ and generally $HCrO_4^-$ is more than $Cr_2O_7^{2-}$. When pH is greater than 6, CrO_4^{2-} is the main form.[5,60] Thus, the effect of pH was investigated. SiO_2–CHO–APBA adsorbent of 20 mg and the other common used adsorbents (SiO_2–NH_2, SiO_2–SH, and SiO_2–EDTA) were separately added into 20 mL 50 mg L^{-1} Cr(VI) solution with pH from 2 to 8. The mixture were shaken for 4 h at room temperature. The supernates were analyzed by UV spectrophotometer and results were shown in Fig. 3(a).

From the data, it was obvious that the absorption of SiO_2–CHO–APBA to Cr(VI) was maximum which was up to 41.55 mg g^{-1} at pH 2. Under acidic conditions, the boronic acid group on

© 2023 The Author(s). Published by the Royal Society of Chemistry

Open Access Article. Published on 23 May 2023. Downloaded on 2/13/2026 7:31:57 AM.
This article is licensed under a Creative Commons Attribution-NonCommercial 3.0 Unported Licence.

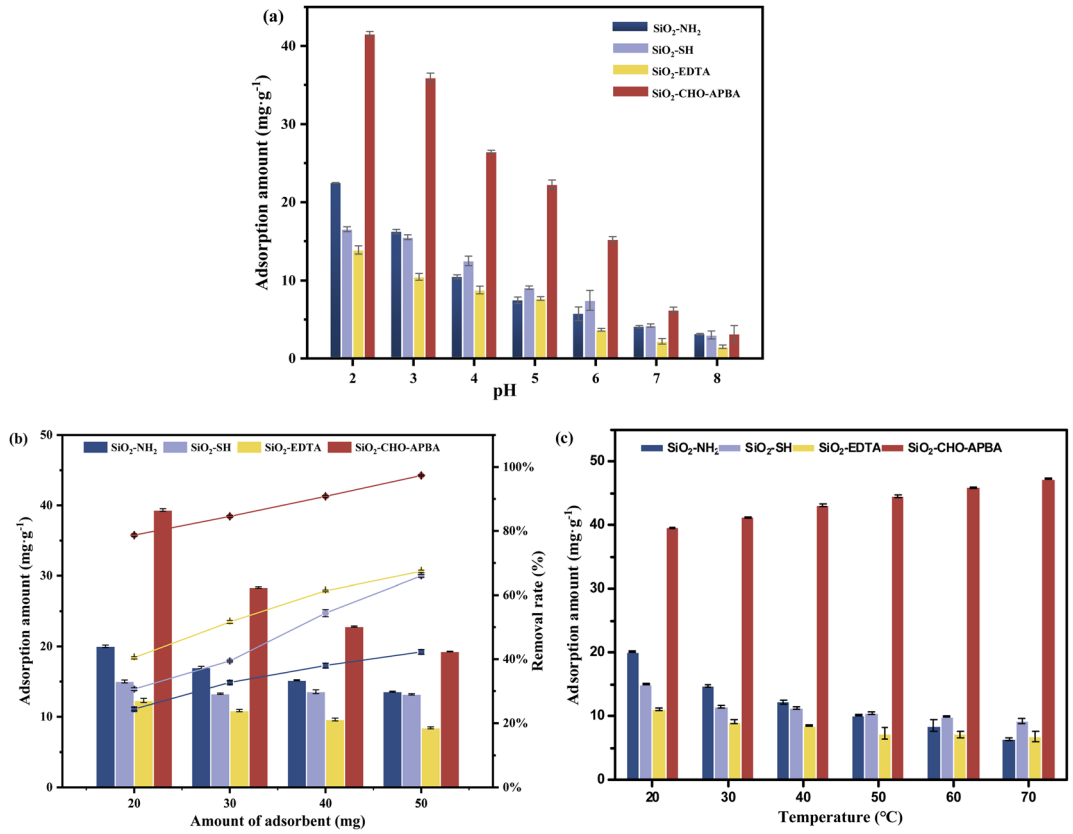

Fig. 3 (a) Effect of pH; (b) effect of amount of adsorbent; (c) effect of temperature on the adsorption of Cr(VI) by four adsorbents.

the surface was positively charged and could be electrostatically attracted to $HCrO_4^-$.[8,34] Meanwhile, the aldehyde group may be important which could reduce $HCrO_4^-$ to Cr^{3+} under acidic conditions. The reaction equation may be as follows.

$$SiO_2–CHO–APBA + 3HCrO_4^- + 8H^+ \rightarrow SiO_2–COOH–[APBA]^+[HcrO_4]^- + 2Cr_3^+ + 5H_2O$$

Under alkaline conditions, neither surface protonation nor reduction reactions were favored.[30] Thus, the adsorption amount decreased significantly to 3.16 mg g^{-1} with pH increase to 8.

The results showed the other three absorbents also had a good adsorption effect under acidic conditions, with the best adsorption at pH 2. However, their maximum were only 1/2 to 1/3 of SiO_2–CHO–APBA, which was significantly low. The adsorption effect also showed a decreasing trend as the acidity decreased. Under low pH, the amino group on the surface of SiO_2–NH_2 was protonated to $-NH_3^+$ of positive charge, which could electrostatically attract the negative ionic $HCrO_4^-$ and formed SiO_2–$[NH_3]^+[HCrO_4]^-$ complex. The best absorption (22.5 mg g^{-1}) of SiO_2–NH_2 to Cr(VI) was obtained at pH 2. With the increase of pH from 3 to 8, the protonation degree of amino group decreases, meanwhile the increasing OH^- would effectively compete amino group with CrO_4^{2-}, which could induce a significant decrease of adsorption amount.[25,41,61] The lowest was only 3.08 mg g^{-1}. Mercaptopropyl in SiO_2–SH has a reducing effect and can reduce chromium from hexavalent to trivalent. Under acidic conditions, the sulfhydryl group could reduce $HCrO_4^-$ to Cr^{3+}.[1,31,41,42] The adsorption effect gradually decreased from 16.54 (pH 2) to 3.44 mg g^{-1} (pH 8) with the decrease of H^+ participation, which was consistent with the results of the existing study.[3] SiO_2–EDTA was rich in carboxyl groups which was differently charged with the change of pH. When the pH was 2, the surface of the material was positively charged and could electrostatically attract $HCrO_4^-$.[15,43] As the pH increases, the surface gradually becomes positively charged and $HCrO_4^-$ could be converted to CrO_4^{2-}.[62] The adsorption free energy change for $HCrO_4^-$ was lower than CrO_4^{2-}, which was more difficult to occur.[17,63] Thus, pH 2 was selected under the following experiments.

3.2.2 Effect of the amount of SiO_2–CHO–APBA. The amount of adsorbent directly affects the adsorption of target. To explore the effect of the amount of adsorbents, 20, 30, 40, or 50 mg adsorbent was added into 20 mL Cr(VI) solution of 50 mg L^{-1} at pH 2 and stood for 4 h. Results were shown in Fig. 3(b). Data indicated the best adsorption was obtained at 20 mg adsorbents. For SiO_2–NH_2, SiO_2–SH, SiO_2–EDTA and SiO_2–CHO–APBA, their adsorption amount to Cr(VI) were 20.01, 15.02, 12.31 and 39.33 mg g^{-1}, respectively. SiO_2–CHO–APBA showed the highest absorption ability to Cr(VI) among the four absorbents. The adsorption amount tended to decrease with the increase of adsorbent amount. The reason maybe the more the

Open Access Article. Published on 23 May 2023. Downloaded on 2/13/2026 7:31:57 AM. This article is licensed under a Creative Commons Attribution-NonCommercial 3.0 Unported Licence.

adsorbent amount, the more sites provided for adsorption and the more favorable the adsorption occurs.[10,64] In contrast, a decrease in the driving force leaded to partial saturation of the active sites on the surface of the adsorbent so that adsorption capacity decreased.[15] To absorb maximum of Cr(VI), 20 mg of SiO_2–CHO–APBA should be selected. The removal rate showed different trends. It obviously increased with adsorbent amount. The removal rate of Cr(VI) for 20–50 mg SiO_2–NH_2, SiO_2–SH, SiO_2–EDTA and SiO_2–CHO–APBA increased from 40.43% to 67.38%, 24.36% to 42.27%, 30.63% to 65.96%, 78.66% to 97.34%, respectively. Among the four absorbents, SiO_2–CHO–APBA also showed the best ability for removal of Cr(VI). The removal rate was more than 97% when its dosage was 50 mg. To pursue the maximum removal rate of Cr(VI), 50 mg of SiO_2–CHO–APBA should be selected. These results verified that SiO_2–CHO–APBA has a significant advantage than the other three common used absorbents.

3.2.3 Effect of temperature on absorption of SiO_2–CHO–APBA to Cr(VI). Temperature may have an effect on the adsorption effect. If adsorption occurs endothermically, the adsorption amount will increase with the temperature rise. On the contrary, it is reversed for exothermic reactions.[22] Thus, temperature was investigated. Each adsorbent of 20 mg was added into 20 mL Cr(VI) solution of 50 mg L^{-1} at pH 2 and stood for 4 h. The temperature was set at 20 °C, 30 °C, 40 °C, 50 °C, 60 °C, or 70 °C. The results were showed in Fig. 4(c). Data showed the adsorption capacities of SiO_2–NH_2, SiO_2–SH and SiO_2–EDTA decreased from 20.05 mg g^{-1} to 6.41 mg g^{-1}, 15.01 mg g^{-1} to 9.18 mg g^{-1}, and 11.06 mg g^{-1} to 6.78 mg g^{-1}, respectively. The decrease trend indicated that adsorption was an exothermic process.[8,15,16,65] In contrast, the adsorption capacity of SiO_2–CHO–APBA increased from 39.54 mg g^{-1} to 47.29 mg g^{-1}. The increased adsorption with temperature indicated that the adsorption was endothermic.[19,25,26,62] It was presumed that the increase in temperature and the acceleration of ion motion lead to the acceleration of electrostatic attraction and reduction reactions. It was consistent with the rate change of a redox reaction with temperature.[6,66] From an economic point of view, the high temperature (70 °C) needs to consume more energy to create the little increase of Cr(VI) adsorption. Thus, 20 °C was selected in the following experiment.

3.2.4 Effect of the time on absorption of SiO_2–CHO–APBA to Cr(VI). Valuable information about the adsorb rate and other details on the overall adsorption process by adsorption kinetics research.[7] To explore the adsorption kinetics, each adsorbent of 20 mg was added into 20 mL Cr(VI) solution of 50 mg L^{-1} at pH 2 and stood at room temperature. The supernatant was sampled at 5, 15, 30, 60, 120, 180, 240, 360, and 720 min and measured the adsorption amount of Cr(VI). Results shown in Fig. 4(a) pointed out that the adsorption started at a fast rate, then the adsorption rate gradually slowed down. After 180 min, adsorption amounts were stable, which indicated that the functional sites of absorbents were involved and the adsorption had reached the equilibrium.[67] The adsorption amounts of SiO_2–NH_2, SiO_2–SH, SiO_2–EDTA and SiO_2–CHO–APBA at 180 min were 19.49, 16.82, 14.14 and 38.60 mg g^{-1}, respectively. SiO_2–CHO–APBA still showed a higher absorption ability than the other absorbents.

To further analyze the Cr(VI) removal performance, the pseudo-first-order and pseudo-second-order kinetic models[23] were exploited to fit the data in Fig. 4(a). The equations of the two models were as follows eqn (6) and (7).

The pseudo-first-order equation is:

$$\ln(Q_e - Q_t) = \ln Q_e - K_1 t \quad (6)$$

The pseudo-second-order equation is:

$$\frac{t}{Q_t} = \frac{t}{Q_e} + \frac{1}{K_2 \times Q_e^2} \quad (7)$$

where K_1 (min^{-1}) and K_2 (g (mg min^{-1})) are the constants of pseudo-first-order rate and pseudo-second-order rate. Q_t (mg g^{-1}) and Q_e (mg g^{-1}) represent the adsorption amount for Cr(VI) at t time and equilibrium, respectively.

The quantitative results including the kinetic constants, equilibrium adsorption capacity, correlation coefficient (R^2) of four adsorbents for Cr(VI) of the two model were shown in the Table 1, Fig. 4(b) and (c). It was found that the pseudo-second order model has a better agreement, all four R^2 were above 0.99. This demonstrated that the adsorption processes of the four absorbents could be well represented by pseudo-second-order (P-S-O) kinetics. In addition, the Q_m calculated by P-S-O (20.84, 17.77, 15.06, and 41.44 mg g^{-1}) were in accordance with the values obtained from the actual experiment (20.59, 17.33, 14.53, and 39.54 mg g^{-1}). The fitted curves of the P-S-O model

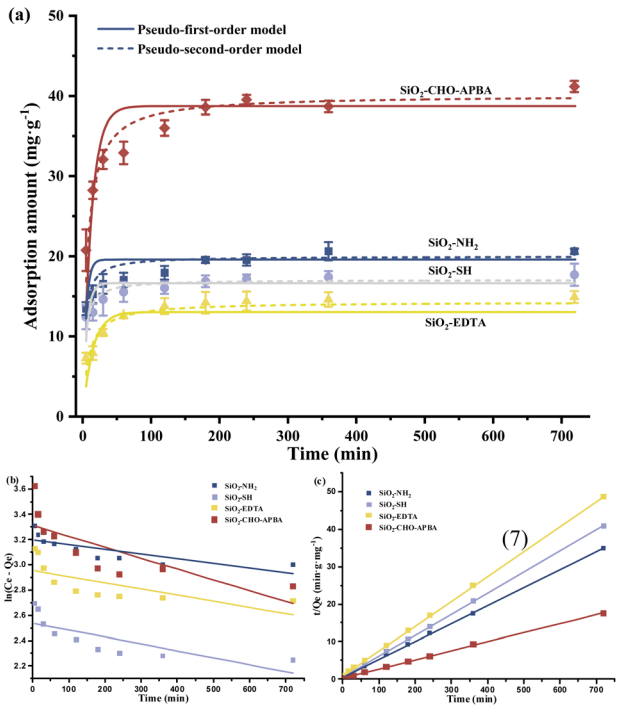

Fig. 4 (a) Adsorption kinetics of Cr(VI) by four adsorbents and the model fitting for pseudo-first-order and pseudo-second-order equation; (b) fitted curves of pseudo-first-order models and (c) pseudo-second-order models of the adsorption.

© 2023 The Author(s). Published by the Royal Society of Chemistry

Open Access Article. Published on 23 May 2023. Downloaded on 2/13/2026 7:31:57 AM. This article is licensed under a Creative Commons Attribution-NonCommercial 3.0 Unported Licence.

Table 1 Pseudo-first-order and pseudo-second-order adsorption kinetics model parameters

	Pseudo-first-order			Pseudo-second-order		
Absorbent	k_1 (min^{-1})	Q_m (mg g^{-1})	R^2	k_1 (g mg^{-1} min^{-1})	Q_m (mg g^{-1})	R^2
SiO_2–NH_2	0.0003788	24.44	0.6407	0.004705	20.84	0.9994
SiO_2–SH	0.0005479	12.65	0.6024	0.007214	17.77	0.9998
SiO_2–EDTA	0.0004884	19.20	0.4952	0.005722	15.06	0.9999
SiO_2–CHO-APBA	0.0008610	27.40	0.5996	0.001984	41.44	0.9990

didn't pass through the origin, indicating that intra-particle diffusion was not the only control step of adsorption,[68] and the adsorption process was dominated by a chemical process.[64]

3.2.5 Effect of concentration and adsorption isotherm. Adsorption isotherm reveals the specific relationship between the degree of deposition and adsorbate concentration on the adsorbent surface at constant temperature.[22] It can be used to not only evaluate the adsorption capacity, but also describe how the adsorbate and adsorbent interact with each other.[69] Thus, the effect of concentration on the adsorption of the adsorbents were investigated at room temperature. Each adsorbent of 20 mg was added into 20 mL of 5, 10, 15, 20, 25, 50, 100, 150, or 200 mg L^{-1} Cr(VI) solution at pH 2 and stood for 4 h. To understand the relationship between Q_e and C_e under equilibrium conditions, the adsorption isotherms of four adsorbents were analyzed by fitting with the Langmuir and Freundlich model.[25]

The Langmuir model assumes a monolayer adsorption and applicable for homogenous surfaces. It assumes each adsorption site has the same activation energy for adsorption, only one molecule can be adsorbed at each site. Freundlich model assumes a multilayer adsorption and applicable for heterogonous surfaces, which means the adsorption sites have different free energy and each site can adsorb multiple molecules.[70] These two models can be expressed using eqn (8) and (9):

$$\frac{C_e}{Q_e} = \frac{1}{bQ_0} + \frac{C_e}{Q_0} \quad (8)$$

$$\ln Q_e = \ln K_f + \frac{1}{n}\ln C_e \quad (9)$$

where Q_e is the equilibrium adsorption capacity (mg g^{-1}), C_e is the concentration of the equilibrium solution (mg mL^{-1}), Q_0 is the saturation adsorption capacity (mg g^{-1}), and b is the adsorption constant represents the adsorption affinity, n is the Freundlich constant represents the ease with which the reaction occurs. When $n > 1$, the adsorption process is easy to occur, when $n < 0.5$ means it is difficult to adsorb, K_f is the binding constant.

The results were shown in Fig. 5(a). In the initial stage (5–100 mg L^{-1}), the adsorption amount increased with the increase of concentration. The adsorption of SiO_2–NH_2, SiO_2–SH, SiO_2–EDTA and SiO_2–CHO–APBA to Cr(VI) of 100 mg L^{-1} were 32.84, 21.72, 18.32 and 53.35 mg g^{-1}, respectively. However, with the further increase of the Cr(VI) concentration, the adsorption amount gradually stabilized, indicating that the sites were all involved in the adsorption process and the adsorption reached the equilibrium. The parameters obtained from fitting two isotherm models with the experimental isotherm data were shown in Table 2. The better fit of the Freundlich model to the experimental data was observed in the case of adsorption of Cr(VI) onto SiO_2–EDTA (see Table 2 and Fig. 5(b)). Good matching of the experimental data to the Freundlich model proved the surface energetic heterogeneity in relation to the adsorbed ions.[1] For SiO_2–NH_2, SiO_2–SH and SiO_2–CHO–APBA, the results indicated the adsorption data were better fitted by the Langmuir isotherm (see Table 2 and Fig. 5(c)), which indicated that the uptake of Cr(VI) by the three adsorbents were dependent on the monolayer adsorption model and the fixed available bonding sites for metals.[3,8,31,41,62] The saturated adsorption amounts of SiO_2–NH_2, SiO_2–SH, SiO_2–EDTA and SiO_2–CHO–APBA calculated by Langmuir isothermal adsorption model are 40.65, 27.17, 29.85 and 58.14 mg g^{-1}, respectively. It was obviously that the adsorption capacity of bi-functional material SiO_2–CHO–APBA was much higher than others, which indicated that simultaneous modification of multiple functional groups could effectively enhance the adsorption capacity.[62]

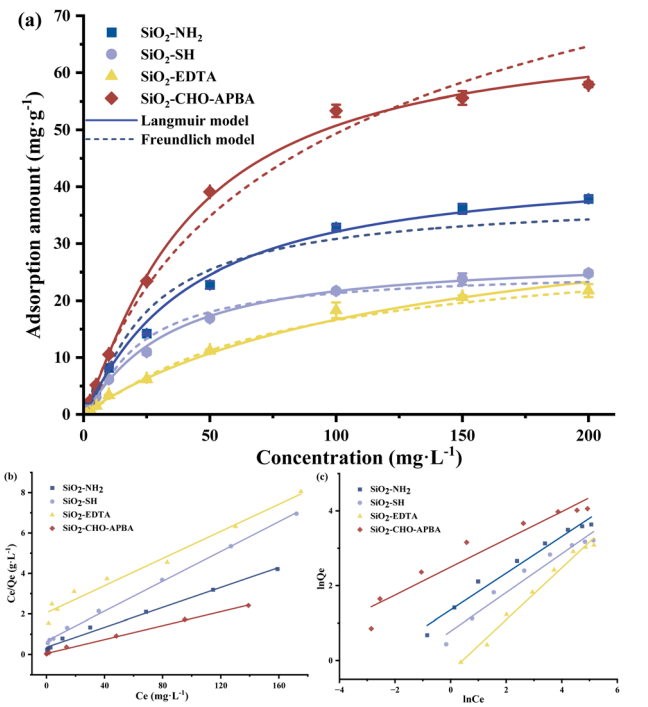

Fig. 5 (a) Adsorption isotherm of Cr(VI) by four adsorbents and the model fitting for Langmuir and Freundlich models; (b) fitted curves of Langmuir model and (c) Freundlich model of the adsorption.

© 2023 The Author(s). Published by the Royal Society of Chemistry

Open Access Article. Published on 23 May 2023. Downloaded on 2/13/2026 7:31:57 AM. This article is licensed under a Creative Commons Attribution-NonCommercial 3.0 Unported Licence.

Table 2 Langmuir and Freundlich isotherm model and parameters

	Langmuir parameters			Freundlich parameters		
Absorbent	Q_0	K_L	R_L^2	K_F	n	R_F^2
SiO_2–NH_2	40.65	0.06900	0.9923	3.8624	2.0404	0.9735
SiO_2–SH	27.17	0.05521	0.9984	2.1795	1.9294	0.9610
SiO_2–EDTA	29.85	0.01630	0.9775	0.7404	1.4413	0.9864
SiO_2–CHO–APBA	58.14	0.3489	0.9983	12.1133	2.6903	0.9278

3.3 Regeneration performance

From the results, it was obvious that SiO_2–CHO–APBA had a significant advantage in the removal of Cr(VI) among the four absorbents. For economic benefits, the regeneration performance of adsorbent is a necessary indicator to evaluate the feasibility of adsorbents utilization in industry.[29,71] Therefore, the regeneration conditions of the material were investigated. SiO_2–CHO–APBA of 20 mg was added into 10 mL of 100 mg L^{-1} Cr(VI) solution at pH 2. After exploring several desorption solutions, 0.2 M Na_3PO_4 showed the highest desorption rate, but it couldn't completely eluted Cr. Because of limitation of silica gel matrix, the stronger base wasn't tried and 0.2 M Na_3PO_4 was selected. After the adsorption equilibrium, the adsorbent was separated from the liquid, and the adsorbed adsorbent was dispersed in 10 mL of Na_3PO_4 to dissociate the adsorbed Cr(VI) species on the surface, then proceed to the next cycle. Five cycles was performed.

The results were shown in Fig. 6. Data showed the state of Cr present in the solution before and after adsorption. When the adsorbent was not added, the solution was entirely Cr(VI). After the addition of SiO_2–CHO–APBA, parts of the Cr(VI) was absorbed in the form of electrostatic attraction to remove Cr(VI). In determination of the supernatant, it was unexpectedly observed both Cr(III) and Cr(VI). The Cr(VI) was the residual Cr(VI) (16.8%) that was not completely adsorbed and Cr(III) (20.4%) was reduced by aldehyde group, in which the similar phenomenon was observed in reduction Cr by hydroxyl group.[29] It indicated that the removal of Cr(VI) occurred under multiple effects. From the cycling results, the adsorption amount was 41.68 mg g^{-1} in the 1st run, decreased significantly to 29.46 mg g^{-1} in the 2nd run, and 21.02 mg g^{-1} in the 3rd run, which showed a decreasing trend and then stabilized. It is presumed that the desorption could only remove the part involved in the electrostatic attraction, and at the same time there was some irreversible adsorption occupying the adsorption sites[29] and the loss of adsorbent.[33,71] After the 3rd cycle, it was presumed that the aldehyde group as a reducing role was depleted so that the adsorption amount gradually stabilized.

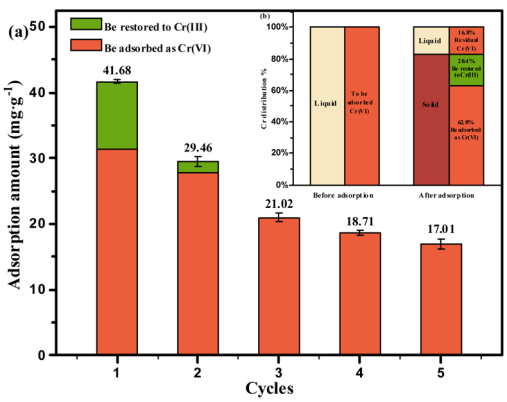

Fig. 6 (a) Recycle adsorption amount of SiO_2–CHO–APBA; (b) the distribution of Cr ion concentrations before and after the adsorption by SiO_2–CHO–APBA.

3.4 Speculation of the adsorption mechanism

The mechanism of Cr(VI) adsorption by SiO_2–CHO–APBA was investigated and results were showed in Fig. 7. Under acidic conditions, Cr(VI) existed as $HCrO_4^-$, while at the same time –B–OH was protonated and existed as $-B-OH_2^+$, which achieved the adsorption of Cr(VI) under electrostatic attraction as Mechanism I shown.[8,34] Mechanism II demonstrated the process of reduction reaction. The aldehyde group was reductive, which was similar to –SH.[3,41] Under acidic conditions, it reduced $HCrO_4^-$ to trivalent chromium which was non-toxic. In the supernatant after adsorption, there were presence of not only Cr(VI), which was not completely adsorbed, but also Cr(III) be restored (see Fig. 6(b)). To verify that the aldehyde group was involved in the removal of Cr(VI), the following experiments were performed. SiO_2–CHO of 20 mg was taken and 10 mL of 100 mg L^{-1} Cr(VI) was added, and the adsorption amount was measured after 4 h. The adsorption amount was calculated according to eqn (3). The adsorption amount of SiO_2–CHO was obtained as 33.48 mg g^{-1}. The adsorption amount of SiO_2–CHO–APBA obtained under the same conditions was 40.49 mg g^{-1}. The results showed that the introduction of bi-functional groups produced a facilitative effect on the adsorption of Cr(VI), and the adsorption amount was increased by about 20.9%. After the solid–liquid separation, 10 mL of 100 mg L^{-1} Cr(VI) was re-added and repeated another twice. The adsorption amounts of Cr(VI) to SiO_2–CHO were 8.24 and 2.39 mg g^{-1}, respectively. The decreasing trend indicated that the participation of aldehyde groups in the adsorption gradually decreased with the increase of the number of repetitions. It proved that the participation of aldehyde group in this process was irreversible. It was consistent with the above results that the adsorption amount of SiO_2–CHO–APBA gradually decreased after repeated use. After drying the aldehyde-based silica gel from three repetitions, it was analyzed using chemical analysis and determined to contain carboxyl groups (0.58 mmol g^{-1}). It further verified the involvement of aldehyde groups in the reduction. In addition, it was speculated that the hydroxyl group in boric acid complexes with oxygen of chromate and held Cr(VI) by hydrogen bonding as shown in mechanism III.

3.5 Application of SiO_2–CHO–APBA in removing Cr(VI) from soil

To investigate the effectiveness of adsorbents in practical applications, four adsorbents were used to remove Cr(VI) in soils. The blank soil sample was thoroughly dried by oven. Soil of 20 g was mixed with 10 mL of 1000 mg L^{-1} Cr(VI) solution, and

© 2023 The Author(s). Published by the Royal Society of Chemistry

Open Access Article. Published on 23 May 2023. Downloaded on 2/13/2026 7:31:57 AM.
This article is licensed under a Creative Commons Attribution-NonCommercial 3.0 Unported Licence.

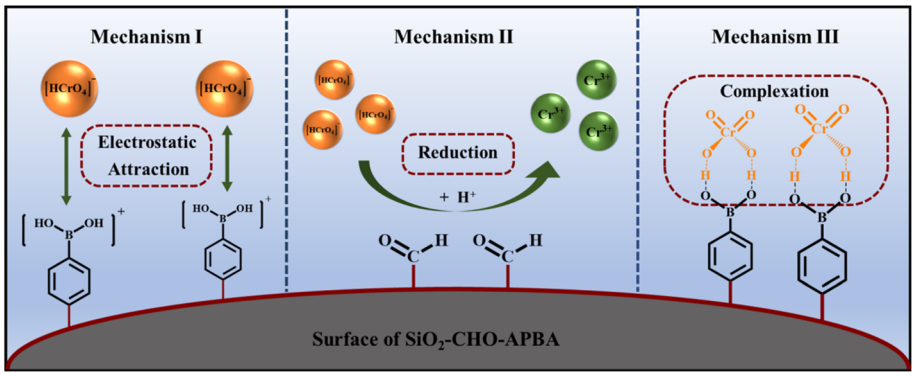

Fig. 7 The speculation of adsorption mechanism between SiO_2–CHO–APBA and Cr(VI).

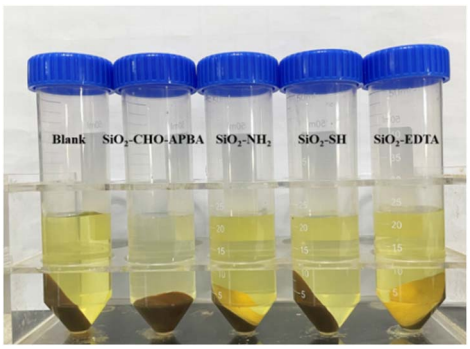

Fig. 8 Before and after adsorption images of Cr(VI) in soils by blank, SiO_2–CHO–APBA, SiO_2–NH_2, SiO_2–SH, and SiO_2–EDTA.

dried to achieve Cr(VI) soil sample. Each adsorbent of 50 mg was mixed with 2 g soil sample containing Cr(VI) and the adsorption was performed under 25 mL pH 2 phosphate buffer for 4 h. The amount of Cr(VI) in the supernatant was measured after centrifugation and the removal rate was calculated.

Result was showed in Fig. 8. It was obvious that all color of the supernatant containing the Cr(VI) and soils became lighter, indicating that the Cr(VI) was successfully absorbed by adsorbents. The supernatant colors from dark to light were SiO_2–EDTA, SiO_2–SH, SiO_2–NH_2 and SiO_2–CHO–APBA, respectively. The removal rates of each adsorbent were 10.35%, 25.04%, 37.90% and 72.48%, indicating that the sequence of absorption ability to Cr(VI) was SiO_2–CHO–APBA, SiO_2–SH, SiO_2–NH_2 and SiO_2–EDTA, which is also consistent with the results of the previous experimental investigations. It demonstrated that SiO_2–CHO–APBA had great application value in removing Cr(VI). If there was an effective reaction to quickly converse back the aldehyde group, it would be huge potential to remove Cr(VI) in industry and agriculture.

4. Conclusion

A bi-functional adsorbent containing an aldehyde group and a phenylboronic acid group was synthesized and applied for the first time to the removal of heavy metals Cr(VI) from aqueous solutions and soils in the environment. FTIR, BET, SEM, TEM, ICP-OES and TGA characterizations were conducted to verify its structure. Four kinds of materials, SiO_2–CHO–APBA, SiO_2–NH_2, SiO_2–SH and SiO_2–EDTA, were used to investigate the optimal adsorption conditions. SiO_2–CHO–APBA exhibited the best adsorption effect than the other three materials. The adsorption results showed that the optimal adsorption conditions were pH 2, temperature 70 °C and 20 mg of adsorbent with the best adsorption capacity and 50 mg of adsorbent with the best removal rate of Cr(VI). The adsorption kinetics showed that the adsorption process of four adsorbents follow pseudo-second-order rate kinetics, and reached adsorption equilibrium after 180 min. The adsorption isotherm was more fitted with Freundlich isotherm model, which indicated that the adsorption process was multilayer adsorption. Regeneration experiments were performed on SiO_2–CHO–APBA. After five cycles, the adsorption amount decreased, indicating that irreversible reactions occurred at some sites of the adsorption process. The adsorption mechanism indicated that the adsorption occurred under the combined effect of reduction of aldehyde groups and electrostatic attraction of phenylboronic acid groups. Applying the four adsorbents to the removal of Cr(VI) from soil, SiO_2–CHO–APBA showed excellent removal ability to Cr(VI) which was superior to that of mono-functional adsorbents. The novel SiO_2–CHO–APBA will have good application prospects in Cr(VI) removal of water and soil samples.

Conflicts of interest

There are no conflicts to declare.

Acknowledgements

The acknowledgments come at the end of an article after the conclusions and before the notes and references. The authors would like to appreciate the financial supports from the National Natural Science Foundation of China (No. 21605112).

References

1 J. Dobrzyńska, *J. Water Process Eng.*, 2021, **40**, 101942–101955.

Open Access Article. Published on 23 May 2023. Downloaded on 2/13/2026 7:31:57 AM. This article is licensed under a Creative Commons Attribution-NonCommercial 3.0 Unported Licence.

2 M. Simone, G. e C. Fernando and d L. P. Maria, *Environ. Health*, 2012, **10**, 227–246.
3 N. Zaitseva, V. Zaitsev and A. Walcarius, *J. Hazard. Mater.*, 2013, **250**, 454–461.
4 J. P. Wise, Jr., J. L. Young, J. Cai and L. Cai, *Environ. Int.*, 2022, **158**, 106877–106894.
5 X. Zhang, W. Fu, Y. Yin, Z. Chen, R. Qiu, M. O. Simonnot and X. Wang, *Bioresour. Technol.*, 2018, **268**, 149–157.
6 W. PAULR and P. TANDCARLD, *Environ. Sci. Technol.*, 1996, **30**, 2470–2477.
7 X. An, L. Zhang, Y. He, W. Zhu and Y. Luo, *Can. J. Chem. Eng.*, 2020, **98**, 1825–1834.
8 A. Kara, E. Demirbel, N. Tekin, B. Osman and N. Besirli, *J. Hazard. Mater.*, 2015, **286**, 612–623.
9 K. Choi, S. Lee, J. O. Park, J. A. Park, S. H. Cho, S. Y. Lee, J. H. Lee and J. W. Choi, *Sci. Rep.*, 2018, **8**, 1438–1447.
10 A. Cimen, E. Karakus and A. Bilgic, *Desalin. Water Treat.*, 2016, **57**, 7219–7231.
11 E. Vaiopoulou and P. Gikas, *Chemosphere*, 2020, **254**, 126876–126878.
12 W. Jiang, Q. Cai, W. Xu, M. Yang, Y. Cai, D. D. Dionysiou and K. E. O'Shea, *Environ. Sci. Technol.*, 2014, **48**, 8078–8085.
13 P. Miretzky and A. F. Cirelli, *J. Hazard. Mater.*, 2010, **180**, 1–19.
14 R. Acharya, A. Lenka and K. Parida, *J. Mol. Liq.*, 2021, **337**, 116487–116501.
15 H. Najafi, N. Asasian-Kolur and S. Sharifian, *J. Mol. Liq.*, 2021, **344**, 117822–117838.
16 S. O. Owalude and A. C. Tella, *J. Basic Appl. Sci.*, 2016, **5**, 377–388.
17 H. Qian, Y. Hu, Y. Liu, M. Zhou and C. Guo, *Mater. Lett.*, 2012, **68**, 174–177.
18 L. N. Tan, N. C. T. Nguyen, A. M. H. Trinh, N. H. N. Do, K. A. Le and P. K. Le, *Sep. Purif. Technol.*, 2023, **304**, 122415–122426.
19 I. Raya, G. Widjaja, Z. H. Mahmood, A. J. Kadhim, K. O. Vladimirovich, Y. F. Mustafa, M. M. Kadhim, T. Mahmudiono, I. Husein and L. Kafi-Ahmadi, *Appl. Phys. A*, 2022, **128**, 167–176.
20 S. Q. Shi, J. K. Yang, S. Liang, M. Y. Li, Q. Gan, K. K. Xiao and J. P. Hu, *Sci. Total Environ.*, 2018, **628**, 499–508.
21 A. K. Mallik, M. A. Moktadir, M. A. Rahman, M. Shahruzzaman and M. M. Rahman, *J. Hazard. Mater.*, 2022, **423**, 127041–127063.
22 A. Bilgic and A. Cimen, *RSC Adv.*, 2019, **9**, 37403–37414.
23 J. Li, M. Li, S. Wang, X. Yang, F. Liu and X. Liu, *Sci. Total Environ.*, 2020, **729**, 139009–139019.
24 L. Ren, Z. Yang, L. Jin, W. Yang, Y. Shi, S. Wang, H. Yi, D. Wei, H. Wang and L. Zhang, *J. Mater. Sci.*, 2019, **55**, 3259–3278.
25 E. H. Jang, S. P. Pack, I. Kim and S. Chung, *Sci. Rep.*, 2020, **10**, 5558–5579.
26 Z. Wei, S. Zhang, X. Wang, S. Long and J. Yang, *J. Appl. Polym. Sci.*, 2021, **138**, 50642–50653.
27 X. S. Wang, L. F. Chen, F. Y. Li, K. L. Chen, W. Y. Wan and Y. J. Tang, *J. Hazard. Mater.*, 2010, **175**, 816–822.
28 J. Xing, J. Li, F. Yang, Y. Fu, J. Huang, Y. Bai and B. Bai, *Sci. Total Environ.*, 2022, **839**, 156367–156377.
29 J. Deng, Y. Liu, H. Li, Z. Huang, X. Qin, J. Huang, X. Zhang, X. Li and Q. Lu, *Sep. Purif. Technol.*, 2022, **295**, 121275–121284.
30 B. Liu, C. Chen, W. Li, H. Liu, L. Liu, S. Deng and Y. Li, *J. Environ. Chem. Eng.*, 2022, **10**, 107433–107440.
31 P. Yang, Y. Shu, Q. Zhuang, Y. Li and J. Gu, *Langmuir*, 2019, **35**, 16226–16233.
32 M. Louis and P. Thomas J, *Chem. Mater.*, 2000, **12**, 188–196.
33 J. Lee, J. H. Kim, K. Choi, H. G. Kim, J. A. Park, S. H. Cho, S. W. Hong, J. H. Lee, J. H. Lee, S. Lee, S. Y. Lee and J. W. Choi, *Sci. Rep.*, 2018, **8**, 12078–12088.
34 W. Kettum, T. T. V. Tran, S. Kongparakul, P. Reubroycharoen, G. Guan, N. Chanlek and C. Samart, *J. Environ. Chem. Eng.*, 2018, **6**, 1147–1154.
35 H. Mao, K. Zhu, B. Li, C. Yao and Y. Kong, *Appl. Surf. Sci.*, 2014, **292**, 1009–1019.
36 V. Kumari, M. Sasidharan and A. Bhaumik, *Dalton Trans.*, 2015, **44**, 1924–1932.
37 B. Veera M, A. Krishnaia, T. Jonathan L and S. Edgar D, *Environ. Sci. Technol.*, 2003, **37**, 4449–4456.
38 A. A. Taha, Y. N. Wu, H. T. Wang and F. T. Li, *J. Mater. Res. Technol.*, 2012, **112**, 10–16.
39 L. Zhu, C. Zhang, Y. Liu, D. Wang and J. Chen, *J. Mater. Chem.*, 2010, **20**, 1553–1559.
40 G. Yang, X. Hu, J. Liang, Q. Huang, J. Dou, J. Tian, F. Deng, M. Liu, X. Zhang and Y. Wei, *J. Hazard. Mater.*, 2021, **419**, 126220–126231.
41 Y. Yang, D. Wang and J. X. Yang, *IOP Conf. Ser. Earth Environ. Sci.*, 2017, **82**, 012074–012083.
42 S. Nataliya, Z. Viladimir and W. Alain, *Environ. Sci. Technol.*, 2008, **42**, 6922–6928.
43 D. Park, Y. S. Yun and J. M. Park, *Chemosphere*, 2005, **60**, 1356–1364.
44 L. Robert Maute and M. L. Owens, *Anal. Chem.*, 1956, **28**, 1312–1314.
45 C. M. de. Sousa, V. L. Cardoso and F. R. X. Batista, *J. Photochem. Photobiol., A*, 2023, **439**, 114602–114609.
46 C. Chen, P. Liu, Y. Li, H. Tian, Y. Zhang, X. Zheng, R. Liu, M. Zhao and X. Huang, *Water Res.*, 2022, **218**, 118502–118511.
47 A. E. David, N. S. Wang, V. C. Yang and A. J. Yang, *J. Biotechnol.*, 2006, **125**, 395–407.
48 F. Esmi, T. Nematian, Z. Salehi, A. A. Khodadadi and A. K. Dalai, *Fuel*, 2021, **291**, 120126–120133.
49 Y. Li, J. He, K. Zhang, T. Liu, Y. Hu, X. Chen, C. Wang, X. Huang, L. Kong and J. Liu, *RSC Adv.*, 2018, **9**, 397–407.
50 S. Çakmak, M. Gümüşderelioğlu and A. Denizli, *React. Funct. Polym.*, 2009, **69**, 586–593.
51 G. Yang, J. Wu, G. Xu and L. Yang, *Colloids Surf., B*, 2010, **78**, 351–356.
52 W. Liu, J. Wang, J. Liu, F. Hou, Q. Wu, C. Wang and Z. Wang, *J. Chromatogr. A*, 2020, **1628**, 461470–461478.
53 Q. Fu, N. Chen, G. Wang and R. Guo, *Macromol. Chem. Phys.*, 2021, **222**, 2100145–2100156.

© 2023 The Author(s). Published by the Royal Society of Chemistry

Open Access Article. Published on 23 May 2023. Downloaded on 2/13/2026 7:31:57 AM.
This article is licensed under a Creative Commons Attribution-NonCommercial 3.0 Unported Licence.

54 M. Thommes, K. Kaneko, A. V. Neimark, J. P. Olivier, F. Rodriguez-Reinoso, J. Rouquerol and K. S. W. Sing, *Pure Appl. Chem.*, 2015, **87**, 1051–1069.
55 B. Perla and Balbuenat and E. G. Keith, *Langmuir*, 1993, **10**, 1801–1814.
56 X. Zheng, Y. Qin, X. Meng, Z. Jin, L. Fan and J. Wang, *J. Chromatogr. A*, 2021, **1639**, 461917–461924.
57 S. Hou, Z. H. Huang, T. Zhu, Y. Tang, Y. Sun, X. Li and F. Shen, *Chemosphere*, 2023, **315**, 137679.
58 S. Liu, L. Liu, Y. Wang, Y. Ouyang, N. Li, Z. Hu and S. Chen, *Int. J. Hydrogen Energy*, 2023, **48**, 9436–9450.
59 Z. Wang, M. C. Liu, Z. Y. Chang and H. B. Li, *RSC Adv.*, 2021, **11**, 25158–25169.
60 A. Zhitkovich, *Chem. Res. Toxicol.*, 2011, **24**, 1617–1629.
61 M. Touihri, F. Guesmi, C. Hannachi, B. Hamrouni, L. Sellaoui, M. Badawi, J. Poch and N. Fiol, *Chem. Eng. J.*, 2021, **416**, 129101–129116.
62 Z. Sun, B. Liu, M. Li, C. Li and S. Zheng, *J. Mater. Res. Technol.*, 2020, **9**, 948–959.
63 A. H. M. G. Hyder, S. A. Begum and N. O. Egiebor, *J. Environ. Chem. Eng.*, 2015, **3**, 1329–1336.
64 T. Wang, Y. Sun, L. Bai, C. Han and X. Sun, *Sep. Purif. Technol.*, 2023, **306**, 122631–122643.
65 T. Vidhyadevi, A. Murugesan, S. S. Kalaivani, M. P. Premkumar, V. Vinoth kumar, L. Ravikumar and S. Sivanesan, *Desalin. Water Treat.*, 2013, **52**, 3477–3488.
66 D. Park, Y. S. Yun, H. W. Lee and J. M. Park, *Bioresour. Technol.*, 2008, **99**, 1141–1147.
67 J. Wen, W. Fu, S. Ding, Y. Zhang and W. Wang, *Chem. Eng. J.*, 2022, **443**, 136510–136521.
68 H. Chen, Y. Gao, A. El-Naggar, N. K. Niazi, C. Sun, S. M. Shaheen, D. Hou, X. Yang, Z. Tang, Z. Liu, H. Hou, W. Chen, J. Rinklebe, M. Pohorely and H. Wang, *J. Hazard. Mater.*, 2022, **425**, 127971–127985.
69 X. Xu, B. Y. Gao, X. Tang, Q. Y. Yue, Q. Q. Zhong and Q. Li, *J. Hazard. Mater.*, 2011, **189**, 420–426.
70 M. Mozaffari Majd, V. Kordzadeh-Kermani, V. Ghalandari, A. Askari and M. Sillanpaa, *Sci. Total Environ.*, 2022, **812**, 151334–151361.
71 G. Yang, X. Hu, J. Liang, Q. Huang, J. Dou, J. Tian, F. Deng, M. Liu, X. Zhang and Y. Wei, *J. Hazard. Mater.*, 2021, **419**, 126220–126231.

© 2023 The Author(s). Published by the Royal Society of Chemistry